DOI: 10.1002/ejic.200801131

Spectral, Structural, and Computational Studies of a New Family of Ruthenium(II) Complexes Containing Substituted 1,10-Phenanthroline Ligands and in situ Electropolymerization of a Phenanthrolineruthenium(II) Complex Bridging Nanogap Gold Electrodes

Wei Huang,*[a] Li Wang,[a] Hirofumi Tanaka,[b] and Takuji Ogawa*[b]

Keywords: Ruthenium / N ligands / Electrochemistry / Electropolymerization / Thin films / Density functional calculations

The synthesis and spectral and structural characterization of a new family of ruthenium(II) complexes containing 3-bromo-, 3,8-dibromo-, 3-(thiophen-2′,2′′-yl)-, and 3,8-(thiophen-2′,2′′-yl)-1,10-phenanthroline (phen) ligands is described. UV/Vis spectroscopy is used to compare the differences between the conjugated π systems in these ligands and their respective $[Ru(bpy)_2]^{2+}$ (bpy = 2,2′-bipyridine) analogs. Density functional theory (DFT) computations have been carried out to compare the energy differences between the single-crystal and the energy-minimized structures for different conformations (*trans*/*trans*, *trans*/*cis* and *cis*/*cis*) of the thiophene rings and their bonded phen ring. The formation of an oligothiophene semiconductor polymer bridging gold electrodes with a gap of around 25 nm gap from Ru^{II} complex **7** by in situ electropolymerization, and its removal, is monitored by scanning electron microscopy (SEM).

1. Introduction

In the late 1970s, conjugated polymers were proclaimed as futuristic new materials that would lead to the next generation of electronic and optical devices.[1,2] Polythiophenes are an important representative class of conjugated polymers as they form environmentally and thermally stable materials that can be used as electrical conductors, polymer light-emitting diodes, transistors, photoresists, antistatic coatings, sensors, batteries, electromagnetic shielding materials, new types of memory devices, nanoswitches, optical modulators and valves, imaging materials, polymer electronic interconnectors, and nanoelectronic and optical devices.[3,4] In this research field, we have recently reported a series of oligothiophene dithiol derivatives and their nanocomposite junctions with active gold nanoparticles between microgapped gold electrodes which exhibit photoresponsive properties.[5]

1,10-Phenanthroline derivatives are one of the important organic functional intermediates as they have found widespread application in coordination chemistry, materials chemistry, analytical chemistry, metalloenzymes, probes of nucleic acids, and redox processes due to their strong chelating ability and good conjugated π systems.[6–8] Halogen substitution at different positions is generally the first synthetic step when modifying the 1,10-phenanthroline ring. To date, there have been several reports on the synthesis of 3-bromo- or 3,8-dibromo-1,10-phenanthroline by different methods and with different yields.[9] Once the bromides have been formed, the conjugated π system of 1,10-phenanthroline can be extended by introducing a variety of functional groups, which means that the energy levels of the resulting molecules can be finely tuned. For example, oligothiophene groups can be introduced at the 3- and 8-positions of 1,10-phenanthroline by a carbon–carbon cross-coupling reaction starting from 3,8-dibromo-1,10-phenanthroline.[10] Furthermore, the α-H atom of the thiophene ring is relatively active for subsequent coupling, polymerization, or substitution reactions. In one of our previous papers, we reported the synthesis, electrochemistry, and electropolymerization of a $[Ru(bpy)_2]^{2+}$ complex with a 3,8-bis(terthiophenyl)-1,10-phenanthroline ligand.[11]

We continue this work here by reporting the crystal structures of 3,8-(thiophen-2′,2′′-yl)-1,10-phenanthroline and four new Ru^{II} complexes bearing 3-bromo-, 3,8-dibromo-, 3-(thiophen-2′,2′′-yl)-, and 3,8-bis(thiophen-2′,2′′-yl)-1,10-phenanthroline ligands (Scheme 1). Density functional theory computations are used to compare the energy differences between the single-crystal and the energy-minimized structures with different conformations (*trans*/*trans*, *trans*/*cis* and *cis*/*cis*) of the thiophene rings and their bonded phen ring. Moreover, preliminary studies are car-

[a] State Key Laboratory of Coordination Chemistry, Nanjing National Laboratory of Microstructures, School of Chemistry and Chemical Engineering, Nanjing University, Nanjing 210093, P. R. China
E-mail: whuang@nju.edu.cn
ogawat@ims.ac.jp
[b] Research Center for Molecular Nanoscience, Institute for Molecular Science, National Institutes of Natural Sciences, 5-1 Higashiyama, Myodaiji-cho, Okazaki, Aichi, 444-8787, Japan

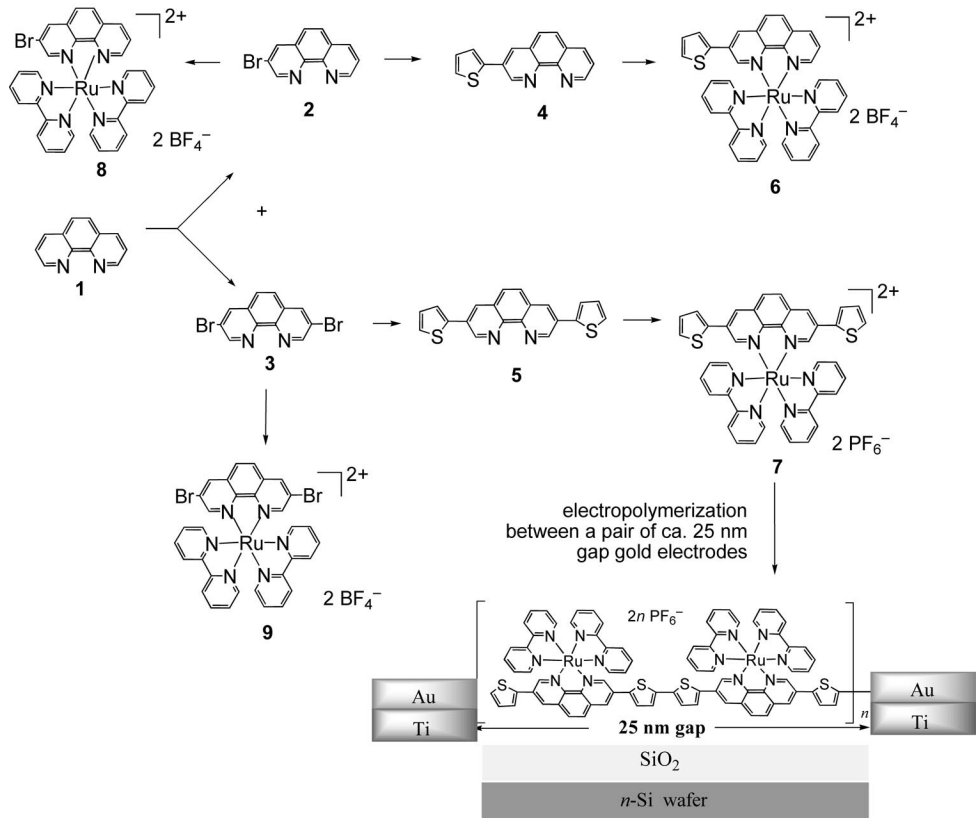

Scheme 1. Schematic illustration showing the preparation of compounds **2**–**9** and polymerization of **7** between a pair of nanogap gold electrodes.

ried out on the electropolymerization of an oligothiophene-based polymer connecting a pair of gold electrodes with a gap of around 25 nm, which has been characterized by SEM images as well as temperature-dependent *I*–*V* curves.

2. Results and Discussion

2.1. Synthesis

Pure 3-bromo-1,10-phenanthroline and 3,8-dibromo-1,10-phenanthroline could be separated by careful silica-gel column chromatography and subsequent recrystallization from a mixture of chloroform and hexane. 3-(Thiophen-2′,2′′-yl)- (**4**) and 3,8-bis(thiophen-2′,2′′-yl)-1,10-phenanthroline (**5**) were prepared by a nickel-catalyzed cross-coupling reaction from 3-bromo- (**2**) and 3,8-dibromo-1,10-phenanthroline (**3**), respectively, in satisfactory yields. An excess of bulky counteranions such as BF_4^- and PF_6^- was used to help precipitate the Ru^{II} complexes. The presence of BF_4^- (complexes **6**, **8**, and **9**) and PF_6^- counterions (complex **7**) was confirmed by FT-IR spectroscopy as tetrafluoroborate and hexafluorophosphate salts have characteristic strong absorptions in the range 1054–1089 and 825–895 cm^{-1}, respectively. The in situ electropolymerization reaction leads to the formation of polymers along the direction of the electric field, where ruthenium(II) complexes are bridged by bithienyl segments due to the formation of a carbon–carbon bond between the α-carbon atoms of the thiophene rings.

2.2. Electronic Spectra

The UV/Vis spectra of **4** and **6** in methanol are shown in Figure 1. Compared with the spectrum of 3-(thiophen-2′-yl)-1,10-phenanthroline, a new broad but weak peak is observed at 450 nm for its $[Ru(bpy)_2]^{2+}$ complex, which can be assigned to the metal–ligand charge transfer (MLCT) absorption between the central Ru^{II} ion and the ligands. In addition, a red shift of 24 nm (from 326 nm in **4** to 350 nm in **6**) is observed for the π→π* transition of the conjugated π system in the ligands upon metal-ion complexation. 3,8-Bis(thiophen-2′,2′′-yl)-1,10-phenanthroline (**5**) has a more delocalized π system than **4**, which means that the influence of the molecular structures on the UV/Vis absorptions can be seen by comparing the corresponding UV/Vis peaks of **5** and its $[Ru(bpy)_2]^{2+}$ complex **7**.[11] The lower energy absorptions are found at 454 nm for the MLCT absorption in **7** and at 340 and 372 nm for the thiophene/phenanthroline π→π* transition in **5** and **7**.

The UV/Vis spectra of **8** and **9** are illustrated in Figure 2. The low energy MLCT bands appear at 449 nm for **8** and 438 nm for **9**, which is consistent with their molecular structures since the bromide atom is more electron-withdrawing.

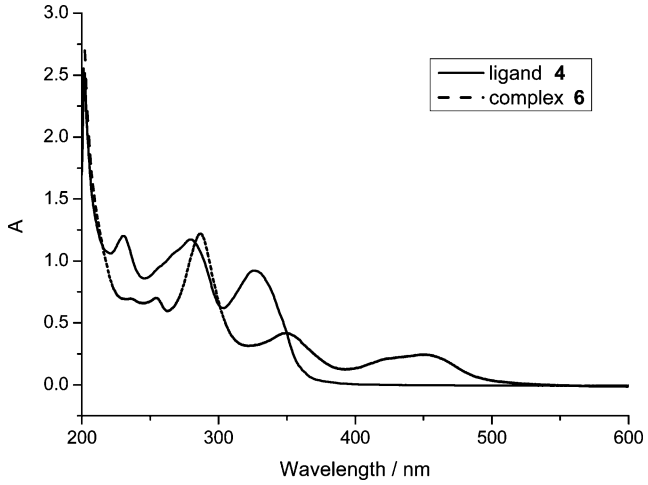

Figure 1. Electronic absorption spectra of ligand **4** (solid line) and complex **6** (dashed line) in methanol.

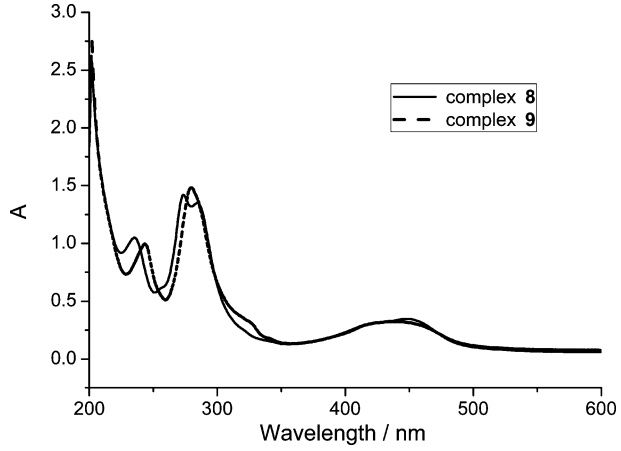

Figure 2. Electronic absorption spectra of complexes **8** (solid line) and **9** (dashed line) in methanol.

2.3. Structural Description of Compound 5

The molecular structure of **5**, with the atom-numbering scheme, is shown in Figure 3. X-ray diffraction studies with **5** indicate that it crystallizes in the triclinic space group $P\bar{1}$ with the chloroform molecule in each asymmetric unit held in place by two C–H···N hydrogen bonds (Table 1) between the hydrogen atom of the chloroform molecule and the two nitrogen atoms of phenanthroline unit. The two side thiophene rings are not coplanar with the central phenanthroline ring but are staggered at each side of the phenanthroline plane with dihedral angles of 14.6° and 15.8°, respectively. The two sulfur atoms of thiophene rings point in the same direction (*trans*/*trans*) as the two nitrogen atoms of the phenanthroline unit.

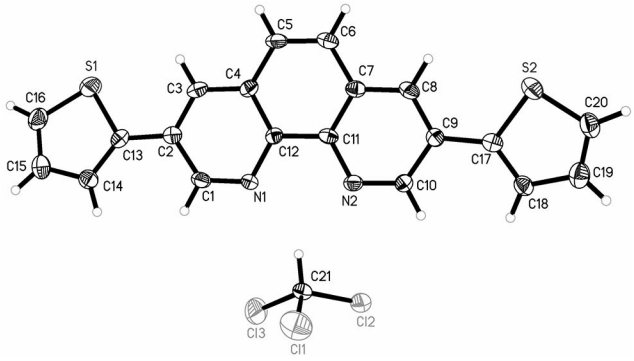

Figure 3. ORTEP diagram (30% thermal probability) of the molecular structure of **5** with the atom-numbering scheme.

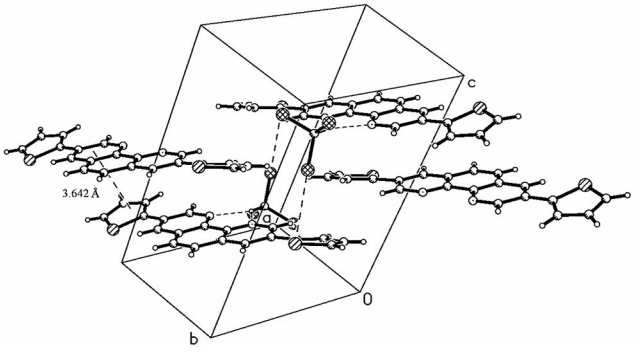

Figure 4. View of the hydrogen bonding and π-π stacking interactions in the packing structure of **5** along with the unit cell. The centroid–centroid separation between the thiophene ring and the side pyridyl ring of phenanthroline is labeled.

Table 1. Main hydrogen-bonding interactions (Å, °) in **5**, **6**, **8** and **9**.

D–H···A	D–H	H···A	D···A	∠DHA	Symmetry transformation
5					
C21–H21···N1	1.00	2.22	3.14(1)	152	1 – *x*, 1 – *y*, 1 – *z*
C21–H21···N2	1.00	2.38	3.17(1)	135	1 – *x*, 1 – *y*, 1 – *z*
6					
O1–H1A···F6	0.85	2.40	2.98(1)	126	1 – *x*, –1/2 + *y*, 3/2 – *z*
O1–H1A···F8	0.85	2.24	2.96(2)	142	1 – *x*, –1/2 + *y*, 3/2 – *z*
8					
O2–H2A···O3	0.85	2.36	3.16(6)	156	
O2–H2B···F6	0.85	2.23	2.86(2)	131	1 – *x*, 1 – *y*, 1 – *z*
O3–H3B···F7	0.85	2.19	2.73(3)	121	1 – *x*, 1 – *y*, 1 – *z*
9					
O2–H2A···F5	0.92	2.49	3.41(4)	175	1 – *x*, 1 – *y*, 1 – *z*

In the crystal packing of **5**, π-π stacking interactions are found between an adjacent thiophene ring and a side-arm pyridyl ring of phenanthroline, with a centroid–centroid separation of 3.642 Å (Figure 4). Additionally, weak S···Cl interactions are observed between the thiophene sulfur atom and the solvent chloroform molecule [3.557 Å].

2.4. Density Functional Theory (DFT) Computational Study for Different Isomers of 4 and 5

DFT calculations were carried out to compare the energy differences between the single-crystal and the energy-minimized structures for **4** and **5** with the thiophene rings in a *trans*/*trans*, *trans*/*cis*, and *cis*/*cis* conformation relative to the phen plane (Scheme 2). The total energy for the single-crystal structure of **5**, where the two sulfur atoms of thiophene rings are in a *trans*/*trans* conformation relative to the two nitrogen atoms of phen unit, is –2356784.36 kJ/mol, while the energy-minimized structure, which has both thiophene rings staggered on each side of the phen plane with a dihedral angle of 14.5°, has a total energy of –2357318.06 kJ/mol. If the two sulfur atoms of the thiophene rings are set to point in the same direction (*cis*/*cis*) as the two nitrogen atoms of the phenanthroline unit, the energy of the ground state optimization is –2357313.66 kJ/mol, with both thiophene rings staggered on each side of the phen plane with a dihedral angle of 21.5°. In contrast, if the two sulfur atoms of the thiophene rings are set on each side of the two nitrogen atoms of the phen unit (*trans*/*cis*), the energy-minimized structure has a total energy of –2357315.96 kJ/mol, with both thiophene rings staggered on each side of the phenanthroline plane with a dihedral angle of 17.8° each.

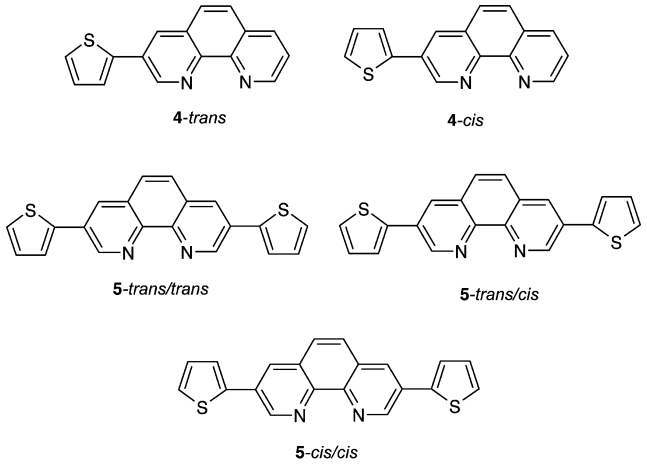

Scheme 2. Schematic illustration of isomers of **4** and **5** in different conformations.

Similarly, if the thiophene ring in **4** is set to a *trans* conformation relative to the two nitrogen atoms of the phen unit, the energy-minimized structure has a total energy of –1928010.84 kJ/mol, with a dihedral angle between the thiophene ring and the phen ring of 18.4°. In contrast, if the thiophene ring is set to the *cis* conformation relative to the two nitrogen atoms of the phen unit, the energy-minimized structure has a total energy of –1928003.73 kJ/mol, with a dihedral angle between the thiophene ring and the phen ring of 21.6°.

Analogous dihedral angles (14.5° for the energy-minimized structure and 14.6° and 15.8° for the single-crystal structure) between the thiophene rings and the phen plane suggest the reliability of our DFT calculations. A large energy gap between the single-crystal structure and the energy-minimized structure in the same *trans*/*trans* configuration reflects the contribution of supramolecular interactions between molecules in the solid state such as hydrogen bonding and π-π stacking. More importantly, the sequence for the thermal stability of energy-minimized structures of **5** in these configurations is *trans*/*trans* > *trans*/*cis* > *cis*/*cis* isomers. However, the energy gaps (2.30 kJ/mol between the *cis*/*cis* and *trans*/*cis* isomers and 2.10 kJ/mol between the *trans*/*cis* and *trans*/*trans* isomers) are not particularly large, which means that all of them are accessible. As for the energy-minimized structures of **4** in the *trans* and *cis* configurations, the *trans* isomer is also somewhat more thermally stable than the *cis* one, although again there is little difference (7.11 kJ/mol) between them. It is likely that the small energy gaps between the *trans* and *cis* isomers of **4** and **5** allow inversion of the thiophene ring due to the free rotation of C–C single bonds between the thiophene rings and the phen ring. These results support the disorder of the thiophene rings found in the $[Ru(bpy)_2]^{2+}$ complexes **6** and **7**. However, the presence of S···Cl interactions between the thiophene sulfur atom and the solvent chloroform molecule in the solid-state structure of **5** may restrict the free rotation of C–C single bonds between the thiophene rings and the phen ring. As a result, the two thiophene rings in **5** are in the *trans*/*trans* conformation relative to the central phen ring and no disorder is observed.

2.5. Structural Description of Complexes 6 and 7

The molecular structures of the cations in **6** and **7**, along with the atom-numbering scheme, are shown in Figure 5. Both cations show similar crystallographic symmetry, with one ethanol molecule present in each asymmetric unit cell. Both ruthenium(II) centers are coordinated by six nitrogen atoms from two bidentate bpy and one bidentate 3-(thiophen-2′,2′′-yl)- or 3,8-bis(thiophen-2′,2′′-yl)-1,10-phenanthroline ligand in a distorted octahedral configuration. There are only slight differences between the bond lengths and bond angles around the central Ru^{II} ions in **6** and **7**.

The dihedral angle between the thiophene ring and its parent phen ring in complex **6** is 19.9°, while the dihedral angles between the phen plane and the two bpy rings are 80.0° and 85.1°, respectively, and that between the two bpy rings is 84.6°. The dihedral angles between the two pyridine rings in two bidentate bpy ligands are 8.0° and 2.5°, respectively. The sulfur atom S1 is best located at the *trans* posi-

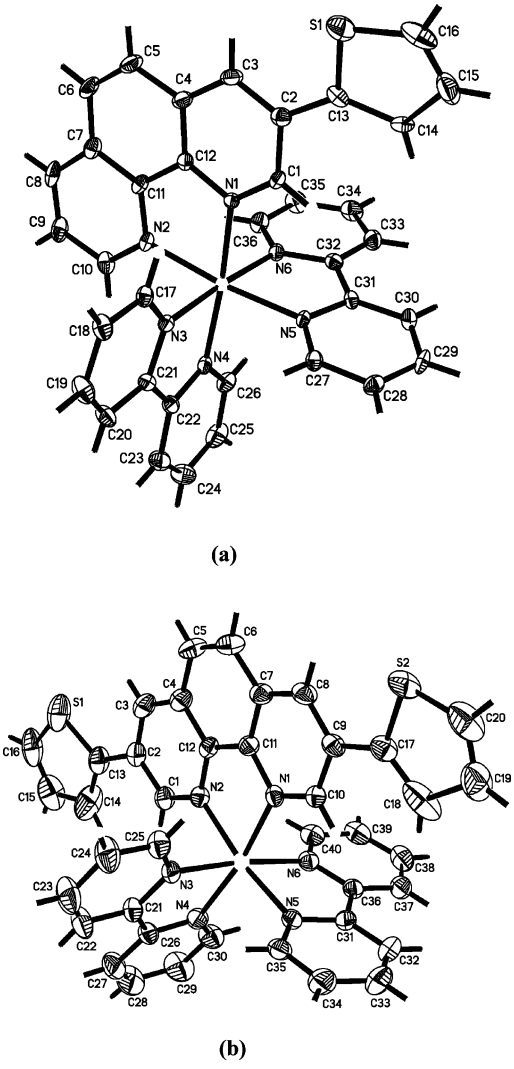

Figure 5. ORTEP diagrams (30% thermal probability) of the molecular structures of **6** (a) and **7** (b) with the atom-numbering scheme. Anions, solvent molecules, and disordered sulfur atoms have been omitted for clarity.

tion of phen ring as the site occupancy factors are 0.765(7)/0.235(7). For comparison, the dihedral angles between the two side thiophene rings and the parent phen ring in complex **7** are lower at 10.6° and 8.1°, respectively. The dihedral angles between the phen plane and the two bpy rings are 80.8° and 89.5°, respectively, and the dihedral angle between the two bpy rings is 72.9°. The two pyridine rings of two bidentate bpy ligands are also essentially coplanar, with dihedral angles of 7.0° and 4.6°. The site occupancy factors are 0.794(10)/0.206(10) for atom S1 and 0.404(9)/0.596(9) for atom S2.

Both complexes contain π-π stacking interactions between adjacent 3-(thiophen-2′,2′′-yl)- or 3,8-bis(thiophen-2′,2′′-yl)-1,10-phenanthroline units, which lead to the formation of layered stacking structures. However, the interlayer separations (3.56 Å for **6** and 3.51 Å for **7**; Figure 6) are different due to the different π-systems of the ligands. To the best of our knowledge, this is the first structural report on thiophene-substituted 1,10-phenanthroline metal complexes.

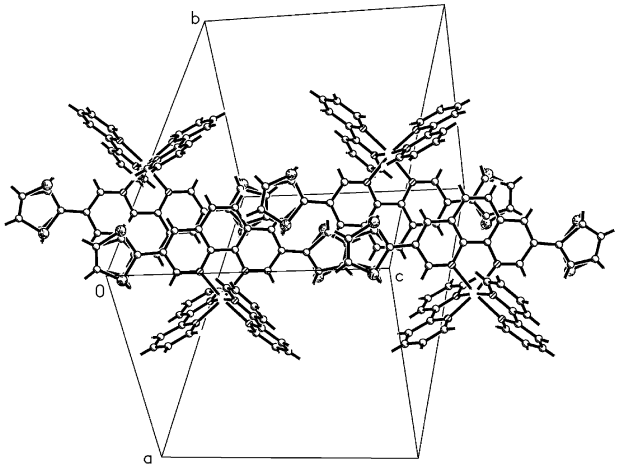

Figure 6. View of the π-π stacking interactions between adjacent molecules in **7** together with the unit cell.

2.6. Structural Description of Complexes 8 and 9

The molecular structures of the cations in **8** and **9**, along with the atom-numbering scheme, are shown in Figure 7. They have the same crystallographic symmetry as the cations in **6** and **7** (monoclinic $P2_1/c$ space group), with one ethanol and two water molecules in **8** and three water molecules in **9** in their asymmetric unit cells. Both ruthenium(II) centers are also coordinated by six nitrogen atoms from one bidentate 3-bromo- or 3,8-dibromo-1,10-phenanthroline and two bidentate bpy ligands in a distorted octahedral configuration. The measured bond lengths and bond angles around the central Ru^{II} ions in **8** and **9** are similar.

The dihedral angles between the phen plane and the two bpy rings in complex **8** are 96.1° and 94.1°, respectively, and the dihedral angle between the two bpy rings is 94.3°. The dihedral angles between two pyridine rings of two bidentate bpy ligands are 7.4° and 7.3°, respectively. In contrast, the dihedral angles between the phen plane and the two bpy rings for complex **9** are 85.7° and 95.3°, and the dihedral angle between the two bpy rings is 98.4°. The dihedral angles between the two pyridine rings of two bidentate bpy ligands are 11.1° and 2.9°, respectively.

A survey of the latest version of the Cambridge Structural Database (Version 5.29)[12] showed that there are no other structures containing 3,8-dibromo-1,10-phenanthroline except for our recent contribution on cadmium(II) complexes.[13a] Furthermore, 3-bromo-1,10-phenanthroline is also rarely involved in structural studies except for one report of an iron(II) complex formulated as [Fe(3-bromo-1,10-phenanthroline)$_3$]$(PF_6)_2$·CH_3CN.[13b] In addition, another two 1,10-phenanthroline complexes multiply substituted by Br at different positions have been documented.[16e,14]

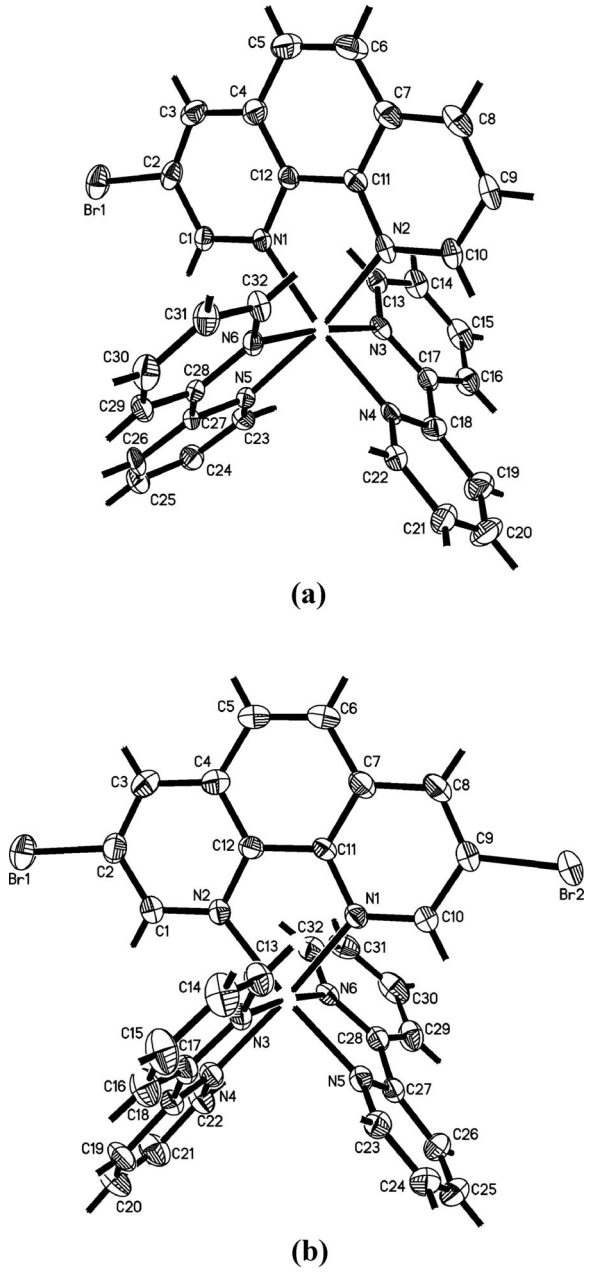

Figure 7. ORTEP diagrams (30% thermal probability) of the molecular structures of **8** (a) and **9** (b) with the atom-numbering scheme. Anions and solvent molecules have been omitted for clarity.

2.7. SEM Images and Temperature-Dependent *I–V* Curves for the Polymer Formed From 7

Electropolymerization has been shown to be a suitable strategy for the preparation of oligothiophene polymers directly between nanogap electrodes as this method avoids the complicated techniques required to manipulate the molecular species for appropriate positioning and contact. As shown in Figure 8, the formation of a polymer from **7** between gold electrodes with a gap of about 25 nm by electropolymerization can clearly be seen in the SEM images before (Figure 8, a) and after electropolymerization (see parts b and c in Figure 8, different magnifications) and that taken after subsequent cleaning with an O_2 plasma (Figure 8, d). The polymer is supposed to grow preferentially oriented along the electric field during the electropolymerization process to form a bunch of wires connecting the two Au electrodes on Si_3N_4 surface. These figures show that the polymer is present between the pair of Au electrodes and that it can be removed by O_2 plasma. However, the SEM images of the bridging polymer in this case are not clear enough, which is probably due to the surface electron charging effect of organic molecules with low conductivity.

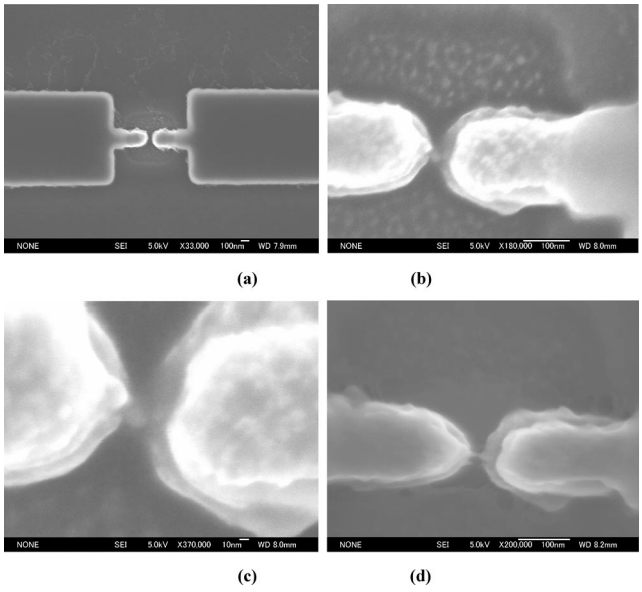

Figure 8. SEM images of the polymer prepared from **7** by electropolymerization between nanogap gold electrodes: a) An Au electrode pair freshly cleaned with O_2 plasma; b) and c) images of the polymer formed between the same gold electrodes taken at different magnifications; d) an SEM image showing partial removal of the polymer between the gold electrodes by O_2 plasma.

In addition to comparing the SEM images of the nanodevices before and after the electropolymerization, a more reliable way to confirm bridging polymer synthesis is to measure the conductivity change between the nanogap Au electrodes in an *I–V* experiment. No current ($<1\times10^{-14}$ A in the voltage range –12 to 12 V) was observed between the bare Au electrodes before the electropolymerization or after O_2 plasma cleaning, whereas a change in conductivity was found upon formation of the semiconductor film. As shown in Figure 9, non-linear, asymmetric temperature-dependent *I–V* curves were found in the range 80–300 K (intervals of 20 K) in the bias voltage range from –12 to 12 V. The likely reason for this is as follows: small changes in interface binding might give an asymmetric response for metal/organic/metal junctions because of nonsymmetric binding even when the electrodes are identical and the molecules are supposedly symmetric, since some charge flow, charge rearrangement, and geometric reorganization, which is voltage-dependent, will occur between the molecule and the metal electrodes. In other words, the different capacitance

of these nanodevices (Schottky barrier between gold electrodes and semiconductor molecules) is likely to influence the symmetry of the *I*–*V* curves at different temperatures.

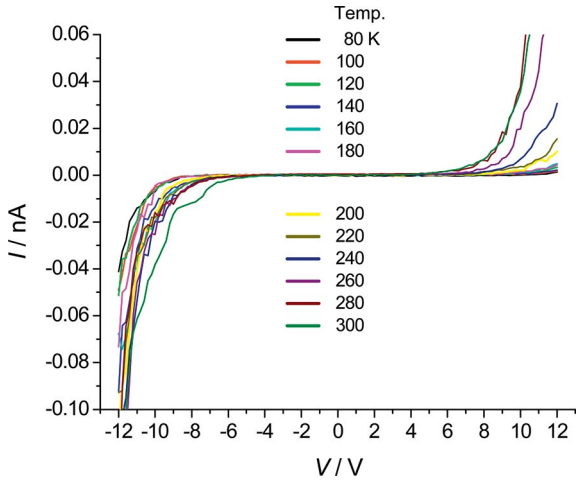

Figure 9. Full range of *I*–*V* curves between 80 and 300 K recorded at intervals of 20 K for the polymer formed between nanogap gold electrodes in the voltage range –12 to 12 V.

The conductivity of the electropolymerized polymer formed from **7** between the nanogap gold electrodes is relatively low, on the order of a few tens of picoamperes. However, the temperature-dependent *I*–*V* curves exhibit typical semiconductor characteristics when comparing the *I*–*V* curves at different temperatures as the overall resistance of the film decreases as the temperature increases. Compared with the *I*–*V* curves of the film prepared from the ruthenium complex of the same 1,10-phenanthroline ligand,[11] the "blockaded" region of the polymer is wider and the conductivity lower at every temperature. This difference can be attributed to the different π conjugated systems of these two species, which affect their bandgaps.

The fixed atom coordinates of **4**, **5**, **6**, and **7**, based on the structural parameters of **5**, **6**, and **7** determined by X-ray diffraction, were used to calculate the HOMO and LUMO. With the MPW1PW91 method and the LanL2DZ basis, the resultant HOMO–LUMO gaps (bandgaps) for ligands **4** and **5** are 4.822 and 4.037 eV, respectively, whereas those for their respective $[Ru(bpy)_2]^{2+}$ complexes **6** and **7** are 3.272 and 3.213 eV. Compared with 3,8-bis(4-mercaptophenyl)-1,10-phenanthroline and its $[Ru(bpy)_2]^{2+}$ complex (4.149 and 2.614 eV),[15] these bandgaps are consistent with their molecular structures and somewhat higher than those of 3,8-bis(terthiophenyl)phenanthroline dithiol and its $[Ru(bpy)_2]^{2+}$ complex (1.770 eV), mainly due to the presence of a different delocalized π-system. The relatively large bandgap value for complex **7** (3.213 eV) may explain the higher resistivity compared with earlier reported Ru^{II} complexes (1.770 eV) under the same experimental conditions.

3. Conclusions

Four six-coordinate $[Ru(bpy)_2]^{2+}$ complexes **6**–**9** containing 3-bromo, 3,8-dibromo, 3-(thiophen-2′,2′′-yl), and 3,8-bis(thiophen-2′,2′′-yl)-1,10-phenanthroline ligands, and the 3,8-bis(thiophen-2′,2′′-yl)-1,10-phenanthroline ligand itself, have been synthesized and structurally characterized. The MLCT and π→π* transitions of the conjugated π system in their UV/Vis spectra have been compared before and after metal complexation and the shifts found to agree well with their molecular structures. The DFT calculations carried out for the single-crystal and energy-minimized structures in different conformations (*trans*/*trans*, *trans*/*cis* and *cis*/*cis*) of thiophene rings and their bonded phen ring explain well the structures found in the solid state and the disorder of the sulfur atoms of the thiophene rings.

All four six-coordinate Ru^{II} complexes crystallize in centrosymmetric space groups, which indicates that the Δ and Λ enantiomers are present in equal amounts in the solid state and that spontaneous resolution does not take place.[17] The coordination chemistry and crystallography reported in this work are valuable because they lead to an estimate for the length of molecule **7** (1.61 nm) and allow us to generate computational models for the DFT studies, especially for the structural comparisons. As far as we are aware, this is the first structural report concerning 3,8-dibromo-1,10-phenanthroline and thiophene-substituted 1,10-phenanthroline ligands and their metal complexes.

SEM has been used to characterize the formation of an oligothiophene polymer, prepared from the Ru^{II} complex **7** by in situ electropolymerization, bridging gold electrodes with a gap of about 25 nm and its subsequent removal by oxygen plasma cleaning. The *I*–*V* curves of this polymer have been measured and its temperature-dependent current-voltage characteristics (80–300 K) investigated. The high resistivity of this nanodevice is thought to originate from the relatively large bandgap value for complex **7**. In order to improve the conductivity of the films bridging the nanogap Au electrodes, studies are currently underway to prepare disulfide-bridged oligothiophene films doped with different amounts of iodine or $NOBF_4$ by in situ oxidation of terminal oligothiophene-based dithiols and to determine their temperature-dependent current-voltage characteristics before and after metal-ion complexation.

Experimental Section

Materials and Measurements: All reagents and solvents were of analytical grade and were used without further purification. The anhydrous solvents were drawn into a syringe under a flow of dry N_2 gas and were transferred directly into the reaction flask to avoid contamination. UV/Vis spectra were recorded with a Shimadzu UV-3150 double-beam spectrophotometer using a Pyrex cell with a path length of 10 mm. Infrared spectra (FT-IR, 4000–400 cm^{-1}) were recorded using a Horiba FT-700 spectrophotometer. ^1H NMR spectra were collected with a Varian Unit 500 MHz spectrometer or a JEOL GSX 270 MHz spectrometer. C, H, and N microanalyses were performed with a Perkin–Elmer 1400C analyzer. Electrospray ionization mass spectra (ESI-MS) were recorded with a Finnigan MAT SSQ 710 mass spectrometer in a scan range of 100–1200 amu. An OLYMPUS BX60M optical microscope was used to check all the electrodes before determination of their *I*–*V* curves. A Yanaco PLASMA ASHER LTA-102 instrument was

used to clean all the electrodes. SEM images were collected with a JEOL JSM-6700F microscope with an acceleration voltage of 5 kV.

The polymer was prepared in situ between gold nanogap electrodes (250 nm wide, gap width ca. 25 nm) by electropolymerization of a saturated solution of **7** in acetonitrile [0.1 M (TBA)ClO_4]. The nanogap electrodes were used as working and counterelectrodes, and a silver wire was employed as a pseudo-reference electrode. The potentials were scanned 10 times in the range –800 to 800 mV. The procedure was repeated after the polarization had been reversed. The samples were then washed thoroughly with methanol and acetone and dried in vacuo. Details of the nanogap electrode fabrication have been published elsewhere.[18] The *I*–*V* curves were collected with an Advantest R6245 2Channels Voltage Current Source Monitor interfaced with a microcomputer through a GPIB-SCSI board and NI-488.2 protocol. Data were acquired using a homemade procedure and Igor Pro 4.0 (Wavemetrics) software. The samples were mounted on top of an antivibration table with a temperature-controlled cryogenic chamber (±0.005 °C). All measurements were carried out under high vacuum ($P < 2.0 \times 10^{-4}$ Pa at room temperature), achieved with a turbo molecular pump, and the samples were cooled using liquid helium as the coolant. The positions of four Pt probes could be adjusted in the *x*, *y*, and *z* directions in order to touch the Au electrodes effectively. Short triaxial cables were used to connect the nanodevices and the *I*–*V* monitor in order to minimize the external noise.

All DFT calculations were carried out with the Gaussian 03 (revision C.02) program suite[19] using the MPW1PW91 method and the LanL2DZ basis set. The fixed atom coordinates of **5**, determined from the structural parameters obtained by X-ray diffraction, were used as the input file for the total energy calculation.

X-ray Data Collection and Solution: All single-crystal samples were covered with glue and mounted on glass fibers for data collection with a Rigaku Mercury CCD area-detector at 100–291 K using graphite-monochromated Mo-K_α radiation (λ = 0.71073 Å). The collected data were reduced with the program Crystalclear[20] and empirical absorption corrections were performed. The original data files generated by Crystalclear were transformed to SHELXTL97 format with the TEXSAN program.[21] The crystal systems were determined by Laue symmetry and the space groups were assigned on the basis of systematic absences using XPREP. The structures were solved by direct methods and refined by least-squares methods on F_o^2 using the SHELXTL PC software package.[22] All non-H atoms were refined anisotropically and all hydrogen atoms were inserted in their calculated positions, assigned fixed isotropic thermal parameters, and allowed to ride on their respective parent atoms. All calculations and molecular graphics were carried out with the SHELXTL PC program package. The sulfur atoms in **6** and **7** as well as some of the fluorine atoms of one of two BF_4^- anions in **6** and **9** and both PF_6^- anions in **7** were refined as disordered with different site occupancy factors. The data for **7** were of relatively low quality, especially for the disordered PF_6^- anions. However, attempts to determine the low-temperature structure were not successful as the crystal appeared to be unstable in the liquid nitrogen stream. A summary of the crystal data, experimental details, and refinement results for **5**–**9** is provided in Table 2. Selected bond lengths and bond angles involving the ruthenium ions and the heteroatoms are given in Table 3, while the hydrogen-bonding interactions are listed in Table 1.

CCDC-670541 (for **5**), -670542 (for **6**), -670543 (for **7**), -670544 (for **8**), -670545 (for **9**) contain the supplementary crystallographic data for this paper. These data can be obtained free of charge from The Cambridge Crystallographic Data Center via www.ccdc.cam.ac.uk/data_request/cif.

Preparation of Compounds: 3-Bromo-1,10-phenanthroline and 3,8-dibromo-1,10-phenanthroline were prepared from 1,10-phenanthroline monohydrate by the literature method.[10] $[Ru(bpy)_2(H_2O)_2](NO_3)_2$, 3,8-bis(thiophen-2′,2′′-yl)-1,10-phenanthroline (**5**) and its Ru^{II} complex bis(2,2′-bipyridine)[3,8-bis(thiophen-2′,2′′-yl)-1,10-phenanthroline]ruthenium(II) dihexafluorophosphate (**7**) were prepared from 3,8-dibromo-1,10-phenanthroline according to a previously described method.[11] Single crystals of **5** suitable for X-ray diffraction were grown from a mixed solution of chloroform and acetone (2:1, v/v) by slow evaporation in air at room temperature. Single crystals of **7** suitable for X-ray diffraction were obtained from a mixed solution of ethanol and water (4:1, v/v) by slow evaporation in air at room temperature.

Synthesis of (3-Thiophen-2′-yl)-1,10-phenanthroline (4): Compound **4** was prepared by a method similar to that for 3,8-bis(thiophen-2′,2′′-yl)-1,10-phenanthroline (**5**) except that 3-bromo-1,10-phenanthroline (25.9 mg, 0.1 mmol) was used as the starting material. Yield 19.4 mg (74%). FT-IR (KBr pellets): $\tilde{\nu}$ = 3058 (m), 1603 (w), 1590 (m), 1557 (w), 1499 (m), 1446 (m), 1428 (s), 1416 (m), 899 (s), 834 (s), 732 (s), 695 (m) cm^{-1}. $C_{16}H_{10}N_2S$ (262.33): calcd. C 73.26, H 3.84, N 10.68; found C 73.22, H 3.95, N 10.64. ^1H NMR (500 MHz, CD_3COCD_3, 298 K, TMS): δ = 9.31 (s, 1 H, phen), 8.99 (d, J = 4.40 Hz, 1 H, phen), 8.51 (s, 1 H, phen), 8.31 (d, J = 8.05 Hz, 1 H, phen), 7.88 (dd, J = 8.75 and 8.80 Hz, 2 H, phen), 7.70 (d, J = 3.65 Hz, 1 H, phen), 7.60 (dd, J = 4.15 and 4.10 Hz, 1 H, thienyl), 7.53 (d, J = 5.15 Hz, 1 H, thienyl), 7.15 (dd, J = 3.65 and 3.40 Hz, 1 H, thienyl) ppm. EI-MS: m/z 262 $[M]^+$. UV/Vis (methanol): λ_{max} = 326, 278, 231 nm.

Synthesis of [Bis(2,2′-bipyridine)(3-thiophen-2′-yl)-1,10-phenanthroline]ruthenium(II) Ditetrafluoroborate (6): Complex **6** was prepared by a method similar to that for the Ru^{II} complex **7** except that (3-thiophen-2′-yl)-1,10-phenanthroline (26.2 mg, 0.1 mmol) was used as the starting material and an excess of $NaBF_4$ was used instead of NH_4PF_6 to precipitate the resulting complex. Yield 58.6 mg (69%). FT-IR (KBr pellet): $\tilde{\nu}$ = 3038 (w), 1638 (m), 1599 (m), 1465 (m), 1440 (s), 1097 (vs), 1060 (vs), 1035 (vs), 841 (m), 770 (s), 732 (m) cm^{-1}. $C_{36}H_{26}B_2F_8N_6RuS$ (849.38): calcd. C 50.91, H 3.09, N 9.89; found C 51.04, H 3.21, N 9.94. ^1H NMR (500 MHz, CD_3COCD_3, 298 K, TMS): δ = 9.01 (d, J = 5.85 Hz, 1 H, phen), 8.92 (d, J = 8.05 Hz, 1 H, phen), 8.90 (d, J = 8.55 Hz, 2 H, bpy), 8.84 (d, J = 8.05 Hz, 2 H, bpy), 8.80 (d, J = 6.80 Hz, 1 H, phen), 8.44 (d, J = 5.40 Hz, 1 H, phen), 8.41 (dd, J = 1.35 and 1.25 Hz, 1 H, phen), 8.34 (d, J = 8.10 Hz, 1 H, phen), 8.31–8.27 (m, 2 H, bpy), 8.19 (d, J = 5.15 Hz, 2 H, bpy), 8.16–8.14 (m, 2 H, bpy), 8.10 (d, J = 5.10 Hz, 1 H, phen), 7.94–7.91 (m, 2 H, bpy), 7.71–7.64 (m, 2 H, bpy), 7.49 (d, J = 2.45 Hz, 2 H, thienyl), 7.43–7.38 (m, 2 H, bpy), 7.19 (dd, J = 3.90 and 3.70 Hz, 1 H, thienyl) ppm. FAB-MS: m/z 763 $[Ru(phen)(bpy)_2BF_4]^+$ (100%). UV/Vis (methanol): λ_{max} = 450, 350, 287, 255, 236 nm. Single crystals of **6** suitable for X-ray diffraction were grown from a mixed solution of ethanol and acetone (2:1, v/v) by slow evaporation in air at room temperature.

Synthesis of Bis(2,2′-bipyridine)(3-bromo-1,10-phenanthroline)ruthenium(II) Ditetrafluoroborate (8): A mixture of stoichiometric amounts of *cis*-bis(2,2′-bipyridine)dichlororuthenium(II) hydrate (484 mg, 1.0 mmol) and 3-bromo-1,10-phenanthroline (259 mg, 1.0 mmol) in 50 mL ethanol was refluxed for 2 h, then the mixture was cooled to room temperature and treated with an excess of aqueous $NaBF_4$ solution. The mixture was concentrated to around 5 mL on a rotary evaporator in order to precipitate the Ru^{II} complex, and then the resulting orange precipitate (**8**) was filtered and

Table 2. Crystal and refinement data for compounds **5**–**9**.

Compound	**5**	**6**	**7**	**8**	**9**
Empirical formula	$C_{21}H_{13}N_2S_2Cl_3$	$RuC_{38}H_{32}N_6SB_2F_8O$	$RuC_{42}H_{34}N_6S_2P_2F_{12}O$	$RuBrC_{34}H_{33}N_6B_2F_8O_3$	$RuBr_2C_{32}H_{28}N_6B_2F_8O_3$
Formula weight	463.80	895.45	1093.88	928.26	979.11
Crystal size [mm]	0.40 × 0.10 × 0.10	0.30 × 0.20 × 0.10	0.40 × 0.30 × 0.20	0.30 × 0.20 × 0.20	0.30 × 0.20 × 0.20
Crystal system	triclinic	monoclinic	monoclinic	monoclinic	monoclinic
Space group	$P\bar{1}$	$P2_1/c$	$P2_1/n$	$P2_1/c$	$P2_1/c$
a [Å]	6.156(1)	23.142(5)	13.830(2)	18.037(4)	10.639(2)
b [Å]	10.669(2)	8.466(2)	21.998(3)	22.244(4)	22.345(5)
c [Å]	15.351(3)	21.288(4)	14.502(2)	8.878(2)	16.159(3)
α [°]	85.60(3)	90	90	90	90
β [°]	88.08(2)	115.93(3)	93.54(1)	90.80(3)	96.43(3)
γ [°]	75.64(3)	90	90	90	90
V [Å^3]	973.7(4)	3750.8(16)	4403.6(11)	3561.4(12)	3817.8(18)
Z, D_{calcd} [Mgm^{-3}]	2, 1.582	4, 1.586	4, 1.650	4, 1.731	4, 1.704
F(000)	472	1808	2200	1856	1928
μ [mm^{-1}]	0.696	0.555	0.617	1.650	2.585
Temperature [K]	100(2)	200(2)	291(2)	150(2)	291(2)
h_{min}/h_{max}	–7/7	–27/23	–16/14	–21/21	–12/12
k_{min}/k_{max}	–10/12	–10/10	–24/26	–26/25	–23/26
l_{min}/l_{max}	–18/18	–23/25	–17/15	–10/9	–19/19
Refinement method	Full-matrix least-squares on F^2	Full-matrix least-squares on F^2	Full-matrix least-squares on F^2	Full-matrix least-squares on F^2	Full-matrix least-squares on F^2
Parameters	253	572	745	496	497
Final R indices [$I > 2\sigma(I)$]	R_1 = 0.0764 wR_2 = 0.1283	R_1 = 0.0838 wR_2 = 0.1512	R_1 = 0.0738 wR_2 = 0.1384	R_1 = 0.0873 wR_2 = 0.1967	R_1 = 0.0655 wR_2 = 0.1449
R indices (all data)	R_1 = 0.0956 wR_2 = 0.1350	R_1 = 0.0978 wR_2 = 0.1564	R_1 = 0.0864 wR_2 = 0.1427	R_1 = 0.0933 wR_2 = 0.1999	R_1 = 0.0733 wR_2 = 0.1486
OF on F^2	1.200	1.194	1.283	1.185	1.190
Res. max./min. electron dens. [e Å^{-3}]	0.403/–0.468	0.523/–0.552	0.575/–0.517	1.633/–1.479	0.672/–0.700

Table 3. Selected bond lengths [Å] and angles [°] in **5**–**9**.

	5		**6**	**7**	**8**	**9**
C2–C13	1.468(7)	Ru1–N1	2.059(6)	2.058(4)	2.061(7)	2.075(5)
C9–C17	1.476(7)	Ru1–N2	2.063(5)	2.080(4)	2.065(5)	2.070(5)
C13–S1	1.735(5)	Ru1–N3	2.056(5)	2.058(4)	2.059(6)	2.057(5)
C16–S1	1.707(5)	Ru1–N4	2.060(7)	2.063(4)	4 2.064(7)	2.065(5)
C17–S2	1.727(5)	Ru1–N5	2.046(5)	2.045(4)	2.062(6)	2.061(5)
C20–S2	1.704(5)	Ru1–N6	2.062(7)	2.053(4)	2.068(2)	2.055(5)
C13–S1–C16	92.1(2)	N1–Ru1–N2	79.7(2)	80.1(1)	79.7(2)	280.0(2)
C17–S2–C20	92.2(2)	N1–Ru1–N3	96.2(2)	94.2(2)	96.5(2)	97.6(2)
		N1–Ru1–N4	174.4(2)	171.0(2)	173.3(2)	174.7(2)
		N1–Ru1–N5	96.0(2)	91.0(1)	93.9(2)	95.5(2)
		N1–Ru1–N6	86.5(2)	89.5(2)	88.0(2)	87.3(2)
		N2–Ru1–N3	86.4(2)	86.5(2)	89.6(2)	87.7(2)
		N2–Ru1–N4	97.7(2)	93.5(2)	95.4(2)	96.4(2)
		N2–Ru1–N5	174.0(3)	170.8(1)	171.7(3)	174.2(2)
		N2–Ru1–N6	96.8(2)	99.1(2)	95.6(2)	97.6(2)
		N3–Ru1–N4	78.7(2)	79.0(2)	78.9(3)	78.3(2)
		N3–Ru1–N5	98.2(2)	96.2(2)	96.5(2)	96.6(2)
		N3–Ru1–N6	176.2(2)	173.8(2)	173.7(2)	173.4(2)
		N4–Ru1–N5	87.0(2)	95.6(2)	91.4(2)	88.4(2)
		N4–Ru1–N6	98.7(2)	97.9(2)	97.0(3)	97.1(2)
		N5–Ru1–N6	78.7(2)	78.7(2)	78.8(2)	78.4(2)

dried under vacuum. Yield 609 mg (72%). FT-IR (KBr pellet): $\tilde{\nu}$ = 3230 (w), 1648 (m), 1577 (m), 1560 (m), 1499 (m), 1420 (s), 1084 (vs), 1060 (vs), 731 (s), 668 (s) cm^{-1}. $C_{32}H_{23}B_2BrF_8N_6Ru{\cdot}C_2H_5OH{\cdot}2H_2O$ (928.25): calcd. C 43.99, H 3.58, N 9.05; found C 44.17, H 3.69, N 9.23. ^{1}H NMR (500 MHz, CD_3COCD_3, 298 K, TMS): δ = 9.07 (dd, J = 1.95 and 1.95 Hz, 1 H, phen), 8.87 (d, J = 1.70 Hz, 1 H, phen), 8.85 (d, J = 4.40 Hz, 2 H, bpy), 8.82 (d, J = 5.65 Hz, 2 H, bpy), 8.81 (d, J = 1.15 Hz, 1 H, phen), 8.48 (d, J = 4.40 Hz, 1 H, phen), 8.45 (dd, J = 1.35 and 1.25 Hz, 1 H, phen), 8.35 (d, J = 9.05 Hz, 1 H, phen), 8.27–8.23 (m, 2 H, bpy), 8.19 (d, J = 5.65 Hz, 2 H, bpy), 8.16–8.10 (m, 2 H, bpy), 8.05 (d, J = 5.60 Hz, 1 H, phen), 7.96–7.86 (m, 2 H, bpy), 7.64–7.62 (m, 2 H, bpy), 7.41–7.37 (m, 2 H, bpy) ppm. UV/Vis (methanol): λ_{max} = 449, 285, 274, 235 nm. ESI-MS: *m*/*z* 759 [Ru(3-bromo-1,10-phenanthroline)(bpy)$_2$BF$_4$]$^+$ (100%). Single crystals of **8** suitable for X-ray diffraction were grown from a mixed solution of ethanol and water (3:1, v/v) by slow evaporation in air at room temperature.

Synthesis of Bis(2,2′-bipyridine)(3,8-dibromo-1,10-phenanthroline)-ruthenium(II) Ditetrafluoroborate (9): A mixture of stoichiometric amounts of *cis*-bis(2,2′-bipyridine)dichlororuthenium(II) hydrate (484 mg, 1.0 mmol) and 3,8-dibromo-1,10-phenanthroline (340 mg, 1.0 mmol) in 50 mL of ethanol was refluxed for 2 h, then the mixture was cooled to room temperature and treated with an excess of aqueous $NaBF_4$ solution. The mixture was concentrated to around 5 mL using a rotary evaporator in order to precipitate the Ru^{II} complex, and then the resulting orange precipitate (**9**) was filtered and dried under vacuum. Yield 740 mg (80%). FT-IR (KBr pellet): $\tilde{\nu}$ = 3397 (w), 3065 (w), 1653 (m), 1636 (m), 1560 (s), 1465 (m), 1437 (s), 1420 (s), 1089 (vs), 1076 (vs), 1054 (vs), 1036 (vs), 939 (m), 889 (m), 768 (s) cm^{-1}. $C_{32}H_{22}B_2Br_2F_8N_6Ru{\cdot}3H_2O$ (979.09): calcd. C 39.26, H 2.88, N 8.58; found C 39.19, H 2.91, N 8.63. ^1H NMR (500 MHz, CD_3COCD_3, 298 K, TMS): δ = 9.08 (d, J = 1.95 Hz, 2 H, phen), 8.85 (d, J = 8.30 Hz, 2 H, bpy), 8.82 (d, J = 8.10 Hz, 2 H, bpy), 8.48 (d, J = 1.95 Hz, 2 H, phen), 8.41 (s, 2 H, phen), 8.27–8.23 (m, 2 H, bpy), 8.18 (d, J = 7.55 Hz, 2 H, bpy), 8.15–8.11 (m, 2 H, bpy), 8.02 (d, J = 5.85 Hz, 2 H, bpy), 7.64–7.62 (m, 2 H, bpy), 7.41–7.38 (m, 2 H, bpy) ppm. UV/Vis (methanol): λ_{max} = 438, 280, 244 nm. ESI-MS: *m*/*z* 838 [Ru(3,8-dibromo-1,10-phenanthroline)$(bpy)_2BF_4]^+$ (100%). Single crystals of **9** suitable for X-ray diffraction determination were grown from a mixed solution of methanol and water in a ratio of 3:1 (*v*/*v*) by slow evaporation in air at room temperature.

Acknowledgments

W. H. acknowledges the Major State Basic Research Development Programs (Nos. 2007CB925101 and 2006CB806104), the National Natural Science Foundation of China (Nos. 20871065 and 20721002). This work is also supported by a Grant-in-Aid for Scientific Research (Nos. 15201028 and 14654135) and for Key-Technology ("Atomic Switch Programmed Device") from the Ministry of Culture, Education, Science Sports, and Technology of Japan.

[1] D. Fichou, *Handbook of Oligo- and Polythiophenes*, Weinheim, Wiley-VCH (Germany), **1999**.
[2] M. A. Reed, T. Lee, *Molecular Nanoelectronics* **2003**, American Scientific Publishers, Los Angeles, California, USA.
[3] T. Skotheim, J. Reynolds, R. Elsenbamer, *Handbook of Conducting Polymers 2nd Edition*, Marcel Dekker, Inc. New York (USA), **1998**.
[4] a) Y. Wada, M. Tsukada, M. Fujihira, K. Matsushige, T. Ogawa, M. Haga, S. Tanaka, *Jpn. J. Appl. Phys.* **2000**, *39*, 3835–3849; b) T. Ogawa, K. Kobayashi, G. Masuda, T. Takase, S. Maeda, *Thin Solid Films* **2001**, *393*, 374–378; c) H. Ozawa, M. Kawao, H. Tanaka, T. Ogawa, *Langmuir* **2007**, *23*, 6365–6371; d) T. Ogawa, H. Ozawa, M. Kawao, H. Tanaka, *J. Mater. Sci: Mater. Electron* **2007**, *18*, 939–942; e) F. Li, J. B. Wiley, *Dalton Trans.* **2008**, 3977–3980.
[5] a) W. Huang, G. Masuda, S. Maeda, H. Tanaka, T. Ogawa, *Chem. Eur. J.* **2006**, *12*, 607–619; b) T. Ogawa, W. Huang, H. Tanaka, *Mol. Cryst. Liq. Cryst.* **2006**, *455*, 299–303.
[6] A. A. Schilt, *Applications of 1,10-Phenanthroline and Related Compounds*, Pergamon, London, **1969**.
[7] P. Tomasik, Z. Ratajewicz, *Pyridine Metal Complexes*, John Wiley & Sons, New York, **1985**.
[8] a) P. G. Sammes, G. Yahioglu, *Chem. Soc. Rev.* **1994**, *23*, 327–334; b) G. Chelucci, R. P. Thummel, *Chem. Rev.* **2002**, *102*, 3129–3170.
[9] a) F. H. Case, *J. Org. Chem.* **1951**, *16*, 941–945; b) Y. Saitoh, T. Yamamoto, *Chem. Lett.* **1995**, 785–786; c) S. Tzalis, Y. Tor, S. Failla, J. S. Siegel, *Tetrahedron Lett.* **1995**, *36*, 3489–3490; d) S. Tzalis, Y. Tor, *Angew. Chem. Int. Ed. Engl.* **1997**, *36*, 2666–2668; e) Y. Saitoh, T. Koizumi, K. Osakada, T. Yamamoto, *Can. J. Chem.* **1997**, *75*, 1337–1339; f) C. D. Buchecker, M. C. Jimenez, J. P. Sauvage, *Tetrahedron Lett.* **1999**, *40*, 3395–3396; g) C. Boldron, M. Pitie, B. Meunier, *Synlett* **2001**, *10*, 1629–1631.
[10] W. Huang, H. Tanaka, T. Ogawa, *J. Phys. Chem. C* **2008**, *112*, 11513–11526.
[11] K. Araki, H. Endo, G. Masuda, T. Ogawa, *Chem. Eur. J.* **2004**, *10*, 3331–3340.
[12] F. H. Allen, *Acta Crystallogr., Sect. B* **2002**, *58*, 380–388.
[13] a) L. Wang, W. You, W. Huang, *J. Mol. Struct.* **2009**, *920*, 270–276; b) K. J. Lee, I. Yoon, S. S. Lee, B. Y. Lee, *Bull. Korean Chem. Soc.* **2002**, *23*, 399–403.
[14] S. Rau, R. Fischer, M. Jager, B. Schafer, S. Meyer, G. Kreisel, H. Gorls, M. Rudolf, W. Henry, J. G. Vos, *Eur. J. Inorg. Chem.* **2004**, 2001–2003.
[15] W. Huang, G. Masuda, S. Maeda, H. Tanaka, H. Hino, T. Ogawa, *Inorg. Chem.* **2008**, *47*, 468–480.
[16] a) Y. Selzer, M. A. Cabassi, T. S. Mayer, D. L. Allara, *J. Am. Chem. Soc.* **2004**, *126*, 4052–4053; b) J. Park, A. N. Pasupathy, J. I. Goldsmith, C. Chang, Y. Yaish, J. R. Petta, M. Rinkoski, J. P. Sethna, H. D. Abruña, P. L. McEuen, D. C. Ralph, *Nature* **2002**, *417*, 722–725; c) H. B. Weber, J. Reichert, F. Weigend, R. Ochs, D. Beckmann, M. Mayor, R. Ahlrichs, H. von Lohneysen, *Chem. Phys.* **2002**, *281*, 113–125; d) M. A. Reed, C. Zhou, C. J. Muller, T. P. Burgin, J. M. Tour, *Science* **1997**, *278*, 252–254; e) J. Tersoff, D. R. Hamman, *Phys. Rev. B* **1985**, *5031*, 805–813.
[17] a) A. von Zelewsky, O. Mamula, *J. Chem. Soc., Dalton Trans.* **2000**, 219–231; b) W. Huang, T. Ogawa, *Polyhedron* **2006**, *25*, 1379–1385.
[18] K. Araki, H. Endo, H. Tanaka, T. Ogawa, *Jpn. J. Appl. Phys.* **2004**, *43*, L634-L636.
[19] M. J. Frisch, G. W. Trucks, H. B. Schlegel, G. E. Scuseria, M. A. Robb, J. R. Cheeseman, J. A. Montgomery Jr., T. Vreven, K. N. Kudin, J. C. Burant, J. M. Millam, S. S. Iyengar, J. Tomasi, V. Barone, B. Mennucci, M. Cossi, G. Scalmani, N. Rega, G. A. Petersson, H. Nakatsuji, M. Hada, M. Ehara, K. Toyota, R. Fukuda, J. Hasegawa, M. Ishida, T. Nakajima, Y. Honda, O. Kitao, H. Nakai, M. Klene, X. Li, J. E. Knox, H. P. Hratchian, J. B. Cross, C. Adamo, J. Jaramillo, R. Gomperts, R. E. Stratmann, O. Yazyev, A. J. Austin, R. Cammi, C. Pomelli, J. W. Ochterski, P. Y. Ayala, K. Morokuma, G. A. Voth, P. Salvador, J. J. Dannenberg, V. G. Zakrzewski, S. Dapprich, A. D. Daniels, M. C. Strain, O. Farkas, D. K. Malick, A. D. Rabuck, K. Raghavachari, J. B. Foresman, J. V. Ortiz, Q. Cui, A. G. Baboul, S. Clifford, J. Cioslowski, B. B. Stefanov, G. Liu, A. Liashenko, P. Piskorz, I. Komaromi, R. L. Martin, D. J. Fox, T. Keith, M. A. Al-Laham, C. Y. Peng, A. Nanayakkara, M. Challacombe, P. M. W. Gill, B. Johnson, W. Chen, M. W. Wong, C. Gonzalez, J. A. Pople, *Gaussian 03*, revision C.02, Gaussian, Inc., Pittsburgh, PA, **2004**.
[20] Molecular structure Coorporation & Rigaku Coorporation, **2001**, *Crystalclear* Version 1.3, MSC, 9009 New Trails Drive, The Woodlands, TX 77381-5209, USA, and Rigaku, Toyko, Japan.
[21] Molecular structure Coorporation & Rigaku Coorporation, **2000**, *TEXSAN*, version 1.11, MSC, 9009 New Trails Drive, The Woodlands, TX 77381-5209, USA, and Rigaku, Toyko, Japan.
[22] *SHELXTL*, version 6.10, Bruker AXS Inc., Madison, Wisconsin, USA.

Received: November 20, 2008
Published Online: February 18, 2009

